Remote Sens. **2015**, *7*, 12478-12502; doi:10.3390/rs70912478

OPEN ACCESS

remote sensing

ISSN 2072-4292

www.mdpi.com/journal/remotesensing

Article

Seasonal Variation of Colored Dissolved Organic Matter in Barataria Bay, Louisiana, Using Combined Landsat and Field Data

Ishan Joshi and Eurico J. D'Sa *

Department of Oceanography and Coastal Sciences, Louisiana State University, Baton Rouge, LA 70803, USA; E-Mail: ijoshi1@tigers.lsu.edu

***** Author to whom correspondence should be addressed; E-Mail: ejdsa@lsu.edu; Tel.: +1-225-578-0212; Fax: +1-225-578-2520.

Academic Editors: Deepak R. Mishra, Sachidananda Mishra and Prasad S. Thenkabail

Received: 27 July 2015 / Accepted: 17 September 2015 / Published: 23 September 2015

Abstract: Coastal bays, such as Barataria Bay, are important transition zones between the terrigenous and marine environments that are also optically complex due to elevated amounts of particulate and dissolved constituents. Monthly field data collected over a period of 15 months in 2010 and 2011 in Barataria Bay were used to develop an empirical band ratio algorithm for the Landsat-5 TM that showed a good correlation with the Colored Dissolved Organic Matter (CDOM) absorption coefficient at 355 nm (a_g355) (R^2 = 0.74). Landsat-derived CDOM maps generally captured the major details of CDOM distribution and seasonal influences, suggesting the potential use of Landsat imagery to monitor biogeochemistry in coastal water environments. An investigation of the seasonal variation in a_g355 conducted using Landsat-derived a_g355 as well as field data suggested the strong influence of seasonality in the different regions of the bay with the marine end members (lower bay) experiencing generally low but highly variable a_g355 and the freshwater end members (upper bay) experiencing high a_g355 with low variability. Barataria Bay experienced a significant increase in a_g355 during the freshwater release at the Davis Pond Freshwater Diversion (DPFD) following the Deep Water Horizon oil spill in 2010 and following the Mississippi River (MR) flood conditions in 2011, resulting in a weak linkage to salinity in comparison to the other seasons. Tree based statistical analysis showed the influence of high river flow conditions, high- and low-pressure systems that appeared to control a_g355 by ~28%, 29% and 43% of the time duration over the study period at the marine end member just outside the bay. An analysis of CDOM variability in 2010 revealed

the strong influence of the MR in controlling CDOM abundance in the lower bay during the high flow conditions, while strong winds associated with cold fronts significantly increase CDOM abundance in the upper bay, thus revealing the important role these events play in the CDOM dynamics of the bay.

Keywords: CDOM; Barataria Bay; Landsat; empirical algorithm

1. Introduction

Colored dissolved organic matter (CDOM) is an optically-active component of total dissolved organic matter (DOM), absorbing light strongly in the UV and visible spectral range, hence influencing light availability in the aquatic environments [1]. Although CDOM protects marine biota from the harmful effects of UV radiation in surface waters [2], it can also adversely affect primary production and the ecosystem health by reducing the quality and the amount of photosynthetically-active radiation (PAR) to phytoplankton [3,4]. In estuarine environments, CDOM is primarily of terrestrial origin and is characterized by the presence of humic acid produced by bacterial decomposition of plant litter, animals and organically rich soils [5], whereas *in-situ* production of CDOM by bacterial and viral decomposition, excretion, grazing, and primary production dominates in oceanic waters [6–9]. Coastal bays are important transition zones between marine and terrigenous environments, supplying elevated amounts of sediments, dissolved organic matter, and nutrients to the coastal waters, making them optically complex and challenging for ocean color remote sensing applications. For example, previous studies [8,10–12] have attributed the errors in satellite-based estimates of chlorophyll-a to elevated levels of CDOM in coastal waters.

Barataria Bay, together with the neighboring Timbalier-Terrebone Bay system, was designated as one of the 28 estuaries of national significance by the Environmental Protection Agency National Estuary Program in 1991 [13]. Barataria Bay, a transition zone between the terrestrial and marine environments, supplies large amounts of organic matter to the shelf waters that may contribute to the summertime hypoxia in the Northern Gulf of Mexico [14–16]. It has also been experiencing significant loss of wetlands due to the effects of sea-level rise, subsidence, waves and anthropogenic activities such as construction of the man-made levee system along the Mississippi River and canal dredging [17–20]. Despite having no direct river input, Barataria Bay still receives small amounts of nutrient-rich river water through small channels and freshwater diversions [19]. Elevated CDOM absorption and change in the *bacterioplankton* community structure in the bay during the freshwater release at Davis Pond Freshwater Diversion (DPFD) coupled with the shorter flushing times (20–30 days), as compared to "normal condition," suggest a more rapid removal of organic matter to the Gulf waters [21,22]. In the winter, the upper part of the bay generally experiences stronger northerly winds that re-suspend sediments in the water column [23] and also likely forces estuarine water out of the bay [24]; conversely, the bay experiences weak winds from the south in the summer and the fall that likely forces saline water into the bay and increases the residence time of CDOM associated with local precipitation, run-off and other fresh water sources in the upper Barataria Basin [25]. Seasonal variability in CDOM absorption and fluorescence characteristics in the bay and shelf waters also suggests a strong terrestrial influence within

Barataria Bay, coupled with river and shelf water exchange near the mouth of the bay [26–28]. The generally shallow water depths of this aquatic system are also likely to make it susceptible to the physical forcings of wind, tides and currents, resulting in the release of CDOM trapped in the bottom sediments by water column mixing [23,29,30]. Since CDOM distribution in Barataria Bay is strongly influenced by the seasonality and the physical forcing, spatial and temporal monitoring of CDOM is necessary to study biogeochemical processes, sources and sinks of DOM, and to improve ocean color estimates of chlorophyll-a. Remote sensing of CDOM done at high spatial and temporal resolution provides an attractive technique to monitor water quality of the smaller water bodies in the coastal environment.

Previous studies have demonstrated the successful use of empirical band ratio algorithms to monitor CDOM absorption using MODIS, SeaWiFS and MERIS sensors in the Northern Gulf of Mexico [10,31–33]; however, these algorithms have been developed using data acquired in the shelf waters and not assessed for the bays. Furthermore, despite the high temporal resolution of sensors such as MODIS, their use in smaller water bodies, such as Barataria Bay, is limited by the coarse spatial resolution (~1 km) of the sensors. Although Landsat is designed to study terrestrial processes and is thus limited by poor spectral and temporal resolution for ocean color applications, its high spatial resolution makes it suitable to investigate the smaller water bodies. Recent studies have demonstrated the potential use of Landsat imagery to monitor CDOM absorption in lakes and rivers, but the algorithm development was limited to imagery from a single month or the same season [34–37]. Neglecting the seasonal component may introduce a significant error to the algorithm's performance, especially in energetic and highly variable environments like bays and estuaries. As bays receive significant amounts of terrestrial DOM/CDOM and are often a major source to the coastal waters, it is hypothesized that Landsat spectral bands that are mainly designed for investigating terrestrial processes could be extended to study CDOM in Barataria Bay. With limited use of Landsat sensor series (Landsat-5 TM, Landsat-7 +ETM, and Landsat-8 OLI) for monitoring CDOM in bays, an important goal of this study was to assess a Landsat-5 TM-based empirical algorithm to monitor CDOM distribution in Barataria Bay. Landsat-5 TM images from different months were used so as to incorporate the effects of seasonality into the algorithm's performance. Spatial and seasonal variation in the CDOM absorption coefficient was investigated to address discrepancy in the match-up comparisons and to examine the effects of meteorological and hydrological factors on CDOM variability in Barataria Bay in 2010 and 2011. The combined use of field measurements, satellite-derived CDOM, in conjunction with meteorological and hydrological parameters, such as winds, man-made fresh water diversion and the Mississippi River (MR) discharge, were examined to assess influences on the seasonal CDOM distribution in different parts of Barataria Bay.

2. Materials and Methods

2.1. Study Area

Barataria Bay, located between Bayou Lafourche to the west and the Mississippi River delta "Belize" to the east (Figure 1), is an irregularly-shaped water body with a surface area of ~1670 km^2 and average daily fresh water inflow of about ~150 $m^3 \cdot s^{-1}$. The Mississippi River was the main source of fresh water and sediments to the Barataria Basin system. However, rainfall became a major source of fresh water following the construction of man-made flood control levees along the river. The basin has also experienced

significant wetland loss due to the negligible inflow of fresh water and sediments from the MR coupled with the effects of anthropogenic stress, sea-level rise, waves, and subsidence [13,17,38]. For most of the year, the northern part of the bay receives freshwater mainly from the Davis Pond Freshwater Diversion (DPFD), including rainfall and run-off [25]. Hence, it can be considered relatively fresher than the southern part, except during the high MR flow conditions when, supported by the southerly winds, river plume reversals could result in significant transport of low salinity waters into the bay [26]. Sampling in Barataria Bay was comprised of 15 stations with Station 1 being the marine end member and Station 15 being the freshwater end member (Figure 1). In this study, Barataria Bay is divided into three sub-sections based on the climatological salinity distribution [22,39] to examine the effect of the meteorological and hydrological factors on the seasonal CDOM optical properties in the bay. The lower bay includes Stations 1–5 (salinity ~21), and those are likely to represent the marine environment, while Stations 11–15 are part of the upper bay (salinity ~7) and mainly characterized by the freshwater environment. Stations 6–10, which were assigned to the central bay, a transition zone (salinity ~13), are likely to have intermediate properties of both the marine and freshwater end members.

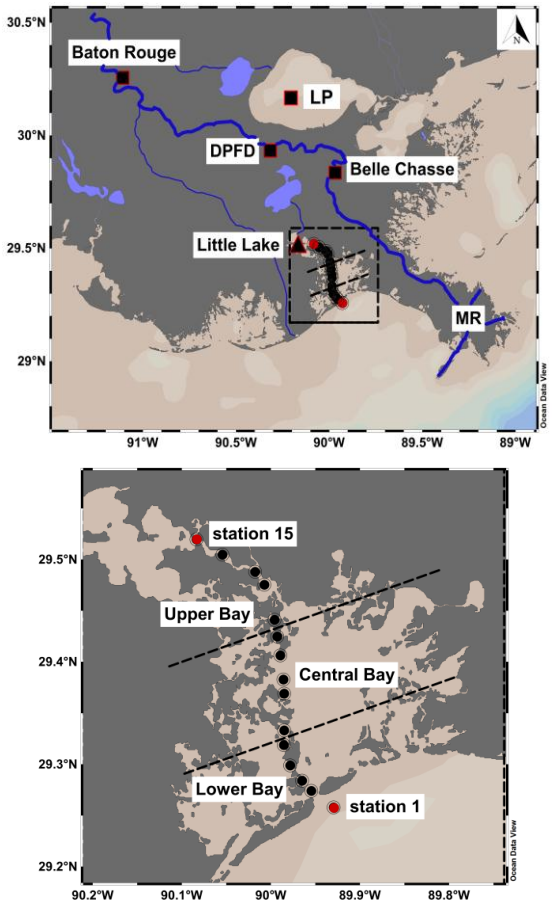

Figure 1. Barataria Bay, Louisiana, USA. Sampling stations are plotted along the transect from the marine end member (Station 1) to the freshwater end member (Station 15). The black squares represent the approximate locations of the Davis Pond Freshwater Diversion (DPFD), Baton Rouge, and Belle Chasse; Little Lake is represented by a triangle. MR is the Mississippi River and LP is Lake Pontchartrain.

2.2. Data Source

Surface water samples were collected at 15 stations from the mouth of Barataria Bay (Station 1) in the Gulf of Mexico to the north (Station 15) in Little Lake during 2010 (10 months) and 2011 (5 months) (Figure 1). Surface temperature and salinity were recorded *in-situ* using a handheld Yellow Springs Instruments (YSI) multi-probe field meter. Water samples were stored in a cooler and brought back to the laboratory on the same day. The samples were immediately filtered using pre-rinsed 0.2-μm Nuclepore membrane filters (Whatman GmbH) and analyzed for optical absorption. Meteorological data (wind speed and wind direction) were acquired from NOAA's National Data Buoy Center (NDBC) at the Grand Isle station (GISL1, 20.265 °N, 89.958 °W) for 2010 and 2011. River discharge information was obtained from the USGS Water Data (USGS) at three locations, namely: DPFD, Baton Rouge, and Belle Chasse. Stations in Baton Rouge and Belle Chasse were selected to demonstrate the difference in MR discharge between the upstream and the downstream locations following the freshwater release through the Bonnet Carré Spillway into Lake Pontchartrain during the high flow MR conditions in 2011. Landsat-5 TM images were ordered and downloaded from the Landsat Data Archive (USGS).

2.3. Absorption Spectroscopy

Absorbance (A) spectra were measured on a Perkin Elmer Lambda-850 double beam spectrophotometer. Following the instrument warm up and samples equilibrated to room temperature, absorbance spectra were obtained between 190 and 750 nm at 2-nm intervals using 1-cm path length quartz cuvette. The cuvette was rinsed twice with Milli-Q water (a Barnstead Nanopure® Model D-50280 purification system with purity of 18.2 MΩ) and once with filtered seawater before each measurement to avoid contamination by the previous sample. The absorption coefficients (a_{CDOM}) were calculated using the following equation,

$$a_{CDOM}(\lambda) = 2.304 \times [A(\lambda)/L] \quad (1)$$

where $A(\lambda)$ is the absorbance at a wavelength λ, and L is the path length in meters. The absorption spectra were corrected for scattering, temperature, and baseline drift by subtracting an average value of absorption between 700 and 750 nm from each spectrum [40]. The exponential decay of the absorption coefficient can be given by the following non-linear equation,

$$a_g(\lambda) = a_g(\lambda_{ref}) \times \exp[-S(\lambda - \lambda_{ref})] \quad (2)$$

where $a_g(\lambda)$ is the amplitude of the CDOM absorption coefficient at any wavelength λ and λ_{ref} is the reference wavelength [41]. The absorption spectra generally represented by a non-linear equation (Equation (2)) were converted to a linear form by the logarithmic transformation of the dependent variable. Then, a least squares regression approach was applied to calculate spectral slope *S* between 275 nm and 295 nm, while the absorption coefficient at 355 nm (a_g355) was used as a quantitative parameter of CDOM [42].

2.4. Landsat Imagery

Landsat-5 TM data were used in this study due to the limitations of the Landsat-7 ETM+ sensor (Scan Line Corrector failure). Landsat-5 TM images for Barataria Bay (Path 22, Row 40) were downloaded

from the USGS Landsat Data Archive. All of the selected images had cloud cover of less than 10% with the study area generally cloud free. As conditions in the bay are likely to change rapidly, the time difference between field and satellite observations should be as small as possible. However, due to the longer re-visit period (16 days) of the Landsat-5 TM, an image selection criterion from 0 to ±5 days of *in-situ* measurements was used to obtain a reasonable sample size for the development and validation of the empirical algorithm. Table 1 shows information about 6 cloud-free images that were used in this analysis. Radiometric calibration was applied to all of the images to convert at-sensor DNs (digital numbers) to at-sensor radiance at each spectral band using the following equation,

$$L_n = C_{0n} + C_{1n} \times DN_n \quad (3)$$

where, C_0 and C_1 are offset and gain coefficients of Landsat-5 TM for the corresponding band n, respectively.

Table 1. Information related to six Landsat-5 TM images obtained under clear sky conditions.

Date of Image Acquisition	Date of *In-Situ* Observation	Difference (in days)	Number of Pixels	Visibility (km)	Sun Zenith Angle
		Training data			
7 October 2010	12 October 2010	+5	13	35.67	41 °
1 April 2011	6 April 2011	+5	8	59.33	35 °
12 February 2011	15 February 2011	+3	15	30.09	51 °
11 November 2011	8 November 2011	−3	14	55.03	51 °
		Total = 50			
		Test data			
8 November 2010	11 November 2011	+ 3	15	55.23	49 °
19 May 2011	24 May 2011	+ 5	13	36.66	28 °
		Total = 28			

The water leaving radiance conveys valuable information about the in-water constituents, but it contributes only about 10% to the at-sensor radiance [43]. The major part of at-sensor radiance is mainly contributed by the atmosphere (aerosols and water vapor), specular reflection of directly transmitted sunlight from the water surface (sun glint), direct reflected radiance from the water surface (sky light) and radiance reflected from whitecaps. The raw at-sensor radiance images were corrected for atmospheric effects using the ENVI v 5.2 (ITT Visual Information Solutions, Inc.) FLAASH (Fast Line of sight Atmospheric Analysis of Spectral Hypercubus) module. FLAASH converts radiometrically-calibrated at-sensor radiance images to surface reflectance images by incorporating the MODTRAN4 radiative transfer code. Landsat-5 TM top-of-atmosphere (TOA) radiance files were converted to FLAASH-compatible units ($mW/cm^2/sr/nm$) by multiplying a scale factor of 0.1. The sensor and flight information, such as sensor type, acquisition date and time, sensor altitude and spatial resolution, were entered manually for each image. This information was supplied with the Landsat L1T product as a separate metadata file (*MTL.txt). The atmospheric model was selected based on the latitude of the study area and the month of image acquisition. This analysis includes the images acquired mainly in the spring, winter and fall seasons; therefore, the selected model was the same for all of the images (mid-latitude winter), except October (tropical). All of the images were corrected for adjacency effects

and processed using the DISORT (Discrete Ordinates Radiative Transfer Program for a Multi-Layered Plane-Parallel Medium) multi-scattering model with 16 streams, 15 cm^{-1} MODTRAN resolution, and Kaufman-Tenre aerosol retrieval with the Landsat spectral bands B4 (0.84 μm) and B7 (2.23 μm). The maritime aerosol model was used with a constant initial visibility of 40 km for all of the images with initial visibility being used only when aerosol is not being retrieved. FLAASH, however, calculates visibility prior to the atmospheric correction (Table 1). Sun glint is another major source of preventable contribution to the TOA radiance and it depends on the surface roughness, wind speed, Sun position and satellite viewing angle. Generally, Sun zenith angles between 30 °and 60 °are optimal for minimizing sun glint [44]. Sun zenith angles are shown in Table 1. The range of sensor viewing angles (6 °–9 °) across the study area indicates a negligible effect of sun glint on the satellite imagery. An average value of 3 × 3 pixels was calculated from the atmospherically-corrected Landsat images at sampling stations using SeaDAS 7.2 (OBPG, NASA) for further analysis; however, 1 × 1 pixel values were used at a few stations located in close proximity to the land.

2.5. Statistical Analysis

Under the influence of various meteorological and hydrological factors, the optical properties, such as a_g355, in Barataria Bay can potentially undergo rapid changes. The relationship between a_g355 and wind forcing, for example, could be strongly non-linear and involve complex interactions that could not be explained by commonly-used statistical modeling approaches. Classification (categorical dependent variable) and regression (numerical dependent variable) trees are the modern statistical techniques for exploring and modeling such a complexity in data [45] and have been widely used in a variety of fields such as medicine [46], agriculture [47], engineering [48] and ecology [49]. Trees explain the variation of a single dependent variable corresponding to one or more explanatory variables by splitting data recursively based on the most influential independent variable. It splits observations into two mutually-exclusive groups based on a threshold value of the most influential explanatory variable by keeping each group as homogenous as possible with a minimum residual sum of squares. The main aim of the tree-based method is to partition the dependent variable into homogenous groups keeping the tree reasonably small [45]. However, the splitting procedure grows oversized trees and can be reduced to the optimal size using the *pre-pruning* and *post-pruning* approaches [45,50,51]. This study utilized a tree-based statistical method to examine the complex relationships between the optical, the hydrological and the meteorological data for investigating the relative importance of various factors, such as wind speed, wind direction, Mississippi River discharge at Belle Chasse and discharge at DPFD on CDOM variability at Station 1, located just outside the bay. Each group is characterized by the means of the dependent variable, group size and the percentage of total data. A decision tree was pruned back to avoid over fitting on data with a suitable complexity parameter and minimum cross-validation error.

In the case of remotely-sensed data, the matchup comparisons between satellite-derived estimates and *in-situ* measurements of CDOM absorption were evaluated using statistical criteria, such as bias (%), root mean square error (RMSE), Pearson's correlation coefficient (r) and R-squared (Table 2). THE two sided t-test was used to examine the relative significance of the freshwater release at DPFD on the variability of a_g355 in Barataria Bay in 2010.

Table 2. Statistical criteria for algorithm evaluation and matchup comparison.

Statistical Estimator	Formula
Absolute Bias (%)	$\left\lvert \frac{\sum_{i=1}^{n}(y_i - x_i)}{\sum_{i=1}^{n} x_i} \right\rvert \times 100$
Root Mean Square Error (RMSE)	$\sqrt{\frac{1}{n}\sum_{i=1}^{n}(y_i - x_i)^2}$
Pearson's correlation coefficient (r)	$\frac{n\sum_{i=1}^{n}(x_i y_i) - (\sum_{i=1}^{n} x_i)(\sum_{i=1}^{n} y_i)}{\sqrt{n(\sum_{i=1}^{n} x_i^2) - (\sum_{i=1}^{n} x_i)^2}\ \sqrt{n(\sum_{i=1}^{n} y_i^2) - (\sum_{i=1}^{n} y_i)^2}}$
R-squared (R^2)	r^2

x_i = field observations; y_i = satellite-derived observations; n = number of observations or pairs.

3. Results and Discussion

3.1. Meteorological and Hydrological Conditions during the Study Period

Many important events in 2010 and 2011 such as the passage of a high-pressure system over Barataria Bay (February 2010), the elevated MR flow (April and May 2010), the large amount of freshwater release at the DPFD (May and July 2010), and the high MR flood conditions (April and May 2011) occurred during the study period. The MR discharge at Baton Rouge and Belle Chasse showed a normal trend with high river discharge during the spring and early summer and low river discharge during the late fall and winter (Figure 2, Panel-1). However, exceptionally high discharge peaks in April and May (2011) represent the MR flood in 2011, which was among the largest and the most damaging flood events in the U.S. The difference between the MR discharge at Baton Rouge and Belle Chasse mainly accounts for the freshwater released at the Bonnet Carré spillway (~7000 $m^3 \cdot s^{-1}$) into Lake Pontchartrain in May 2011. Although the bay has been disconnected from the MR by construction of man-made levees, resulting in the loss of direct sediment and fresh water inputs into the bay [13,17,20,38], diversion flows and the exchange of fresher river water through the passes of the inner shelf waters can still influence the bay waters [21,52].

As a wetland restoration effort, the Davis Pond Freshwater Diversion (DPFD) (Figure 1) has been constructed to supply sediment laden Mississippi River water and to reduce the effects of salt water intrusion on the wetland ecosystem [19,25]. Following the Deep Water Horizon (BP) oil spill in 2010, the DPFD was opened to divert MR water to the bay to minimize the impacts of crude oil on the wetlands. The remarkable change in water discharge at the DPFD is illustrated in Figure 2 (Panel-2) when a mean daily discharge of 47.9 ± 17.7 $m^3 \cdot s^{-1}$ (average of 119 days since 1 January 2010) increased to the mean of 196.38 ± 38.9 $m^3 \cdot s^{-1}$ following the opening of the DPFD to its full capacity of 300 $m^3 \cdot s^{-1}$ on 10 May, 2010, and peak daily discharge (~275 $m^3 \cdot s^{-1}$) occurred on the following day. The mean daily discharge during the period of 70 days was 75% higher than the "normal condition". Discharge was reduced to 116 $m^3 \cdot s^{-1}$ on 8 July 2010.

Wind speed time- series showed a normal trend with stronger winds in the winter and early spring and relatively weaker winds in the summer and fall seasons (Figure 2, Panel-3). The bay experienced quite erratic wind directions with large variability in the winter and the spring and small variability in the summer and fall (Figure 2, Panel-3). Time-series of atmospheric pressure and air temperature (**not**

shown) indicated that the bay was influenced by a high- pressure system and associated cold front passage in late February (22–28 February, 2010), with low air and water temperatures recorded near the marine stations. A relatively weak high pressure system with elevated northerly winds was recorded in 11 November 2010 (Figure 2, Panel-3).

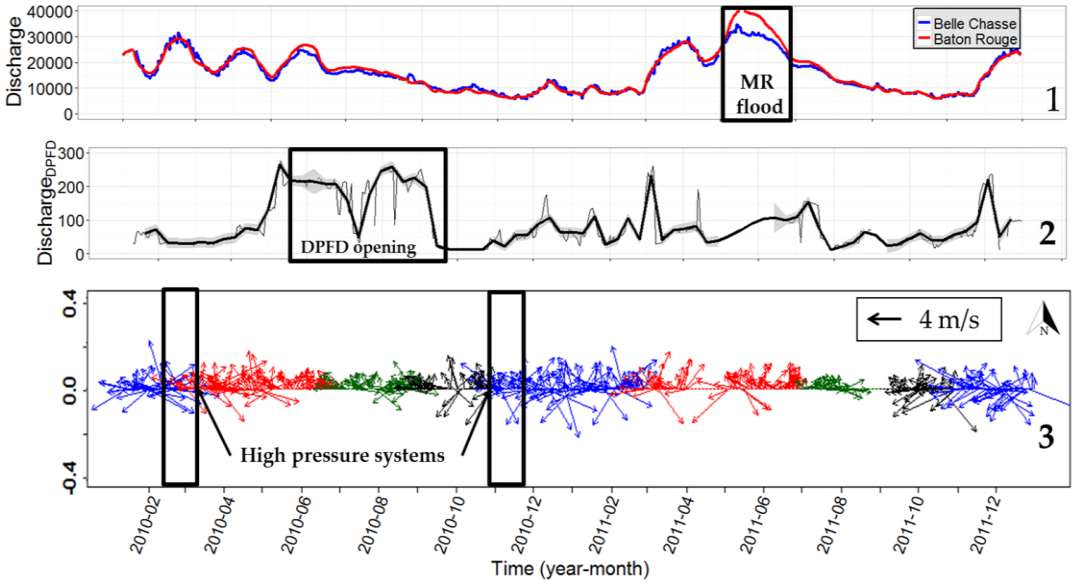

Figure 2. Mean daily discharge ($m^3 \cdot s^{-1}$) of the Mississippi River at Baton Rouge (red line) and Belle Chasse (blue line) (**1**), mean daily discharge ($m^3 \cdot s^{-1}$) at Davis Pond Freshwater Diversion (DPFD) (**2**), mean daily wind speed (ms^{-1}) and mean daily wind direction (in degrees from the North) (**3**). Black boxes represent the MR flood—The Mississippi River flood condition (May 2011) (1), DPFD opening—A large amount of freshwater release at Davis Pond Freshwater Diversion (April and July, 2010) (2), and the evidences of the high-pressure systems (e.g., cold fronts) during the field observations (February and November, 2010) (panel-3); In (3), the blue, red, green, and black colors represent the winter (November, December, January, and February), the spring (March, April, May, and June), the summer (July and August) and the fall (September and October), respectively.

3.2. CDOM Optical Properties: Field Observations

3.2.1. Spatial and Seasonal Assessment

The bay water was characterized by the mean surface salinity gradients from the marine (Station 1) to the freshwater (Station 15) end members that ranged from 12.04 ±4.23 to 7.18 ±5.73 in the spring, 24.26 ±0.91 to 0.31 ±0.30 in the summer, 23.81 ±2.47 to 5.35 ±0.92 in the fall, and 23.75 ±5.86 to 7.65 ± 5.23 in the winter, respectively (Figure 3a, Table 3). The salinity gradient was relatively weak in the spring indicating the influence of freshwater along the transect, whereas the strong gradients in the fall, winter and summer seasons could be attributed to the reduced effects of the freshwater sources in Barataria Bay. Interestingly, the northern region of the bay was relatively fresh (mean salinity:1.2 ± 0.9 (N = 5), Upper bay) during the summer months, suggesting inputs of freshwater despite low river flow condition and small amounts of diverted freshwater into Barataria Bay (Figure 3a).

Mean surface water temperatures remained stable at all stations with warm temperatures of 30.05 ± 0.75 ℃ to 29.8 ℃ in the summer and the cold temperatures of 16.6 ± 3.69 ℃ to 15.76 ± 3.34 ℃ in the winter from the marine to freshwater stations; however, they were slightly reduced (mean difference = 5%) towards the freshwater end member in the winter and slightly increased (mean difference = 12%) towards the freshwater end member in the spring (blue and green lines in Figure 3b; Table 3). Interestingly, the mean surface temperature together with salinity indicated the influence of the freshwater sources (e.g., the MR plume) in the lower bay in the spring. The differences in temperature of the upper and lower bays likely reflected the relatively stronger effects of the cold air temperatures from fresh to the marine end members in the winter (Figure 3b).

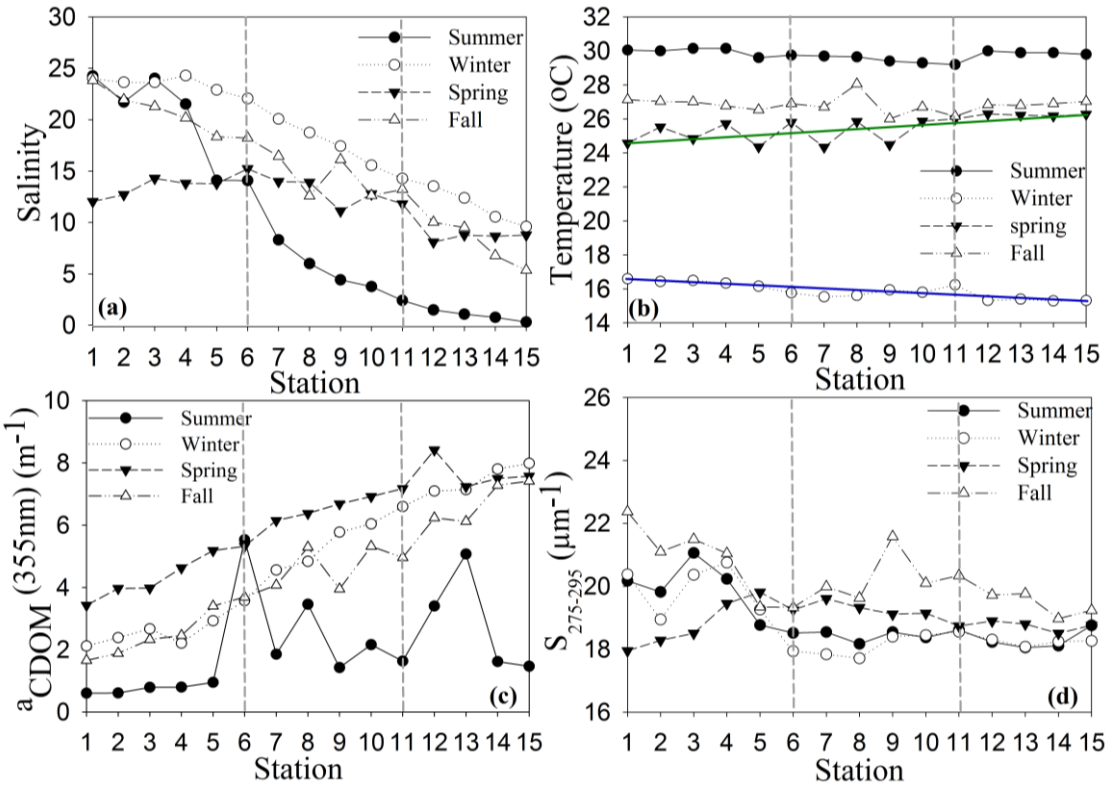

Figure 3. Mean (**a**) salinity, (**b**) temperature (solid lines represent trends), (**c**) CDOM absorption coefficient (a_g355), and (**d**) CDOM spectral slope ($S_{275–295}$) shown for Stations 1–15 (marine to freshwater end member) for summer (filled circles), winter (open circles), spring (inverted triangles) and fall (open triangle). Vertical dashed lines represent the different regions in Barataria Bay, namely: lower bay (Stations 1–5), central bay (Stations 6–10) and upper bay (Stations 11–15).

Mean a_g355 from the freshwater to marine end member stations decreased gradually from 7.41 ± 0.63 m^{-1} to 3.42 ± 0.35 m^{-1} in the spring, 7.47 ± 1.35 m^{-1} to 0.61 ± 0.40 m^{-1} in the summer, 6.41 ± 0.98 m^{-1} to 1.65 ± 0.36 m^{-1} in the fall, and 7.98 ± 1.8 m^{-1} to 2.11 ± 0.77 m^{-1} in the winter, respectively (Figure 3c; Table 3). In the lower bay, high a_g355 (4.2 ± 1.1 m^{-1}) was apparent in the spring with approximately 55%, 75% and 68% higher values compared to the summer, the fall and the winter, respectively. The difference of mean a_g355 between the winter (8.4 ± 4.0 m^{-1}) and the spring (7.6 ± 0.7 m^{-1}) was not significant (t-test: $p > 0.05$) in the upper bay; however, the large variability (SD = 4.0 m^{-1}) could most likely be attributed

to the variation in CDOM sources (e.g., bottom resuspension) associated with frequent and stronger frontal passages during this time of the year.

CDOM spectral slopes ($S_{275–295}$) near the marine end member were also more variable than the freshwater end member, being 17.94 ± 0.68 μm^{-1} in the spring, 20.17 ± 0.84 μm^{-1} in the summer, 22.42 ± 0.97 μm^{-1} in the fall, and 20.37 ± 2.87 μm^{-1} in the winter, respectively (Figure 3d; Table 3). Previous studies in the northern Gulf of Mexico [53] and the Delaware estuary [54] showed similar slopes (15–40 μm^{-1}) and (16–21 μm^{-1}) in the coastal and estuarine environments, respectively. In the spring, low salinity in the lower bay along with highest a_g355 and lowest mean spectral slope suggest the strong influence of fresh MR water that appears, from the salinity trends, to extend into the central and possibly into the upper bay (Figure 3). In contrast, high salinity in the lower bay during summer along with lowest a_g355, but relatively high spectral slope (20.17 ± 0.84 μm^{-1}) with similar patterns during fall suggest strong degradation of CDOM likely by photo-bleaching, due to increased solar insolation and reduced periods of strong winds in the summer and fall [3,55]. The spectral slopes were not significantly different near the freshwater end member, likely indicating similar CDOM sources influenced by the different hydrological and meteorological factors (Table 3, Figure 3d).

The spatial-seasonal analysis showed that the different parts of Barataria Bay were influenced by a variety of factors in different seasons, possibly the MR water in the lower bay and CDOM-rich freshwater, precipitation/run-off and strong winds in the upper bay. In the lower bay, salinity, a_g355 and $S_{275–295}$ were highly variable throughout the study period, whereas lower variability was observed in the upper bay except during the summer. The effects of various hydrological and meteorological events are investigated in detail in the following sections.

Table 3. Salinity, temperature, a_g355 and $S_{275–295}$ (mean ± SD) at two stations (1 and 15) during spring, summer, fall and winter.

Season	Station-01 (South of Barataria Bay)			Station-15 (North of Barataria Bay)		
	Salinity (PSU)	Temperature (℃)	a_g355 (m^{-1}) ($S_{275–295}$ (μm^{-1}))	Salinity (PSU)	Temperature (℃)	a_g355 (m^{-1}) ($S_{275–295}$ (μm^{-1}))
Spring	12.04 ± 4.23	24.58 ± 3.09	3.42 ± 0.35 (17.94 ± 0.68)	7.18 ± 5.73	27.94 ± 3.40	7.41 ± 0.63 (18.76 ± 0.52)
Summer	24.26 ± 0.91	30.05 ± 0.75	0.61 ± 0.40 (20.17 ± 0.84)	0.31 ± 0.30	29.8	7.47 ± 1.35 (18.75 ± 0.27)
Fall	23.81 ± 2.47	27.13 ± 1.62	1.65 ± 0.36 (22.42 ± 0.97)	5.35 ± 0.92	27.03 ± 2.35	6.41 ± 0.98 (19.36 ± 1.24)
Winter	23.75 ± 5.86	16.6 ± 3.69	2.11 ± 0.77 (20.37 ± 2.87)	7.65 ± 5.23	15.76 ± 3.34	7.98 ± 1.8 (18.26 ± 1.30)

3.2.2. a_g355-Salinity and $S_{275–295}$-Salinity Relationships

a_g355-salinity and $S_{275–295}$-salinity relationships are illustrated in Figures 4 and 5, respectively. A general trend of decreasing CDOM with increasing salinity was evident in all seasons with a strong linear conservative relationship in the summer and the fall ($R^2 > 0.9$). A very weak relationship observed during the spring ($R^2 = 0.16$) as well as a relatively robust relationship in the winter (Figure 4a,d) between CDOM absorption and salinity is further examined in the context of the hydrological and meteorological events discussed earlier that may have influenced the CDOM optical properties in the bay. During spring, an overall lower range in salinity in the bay waters in comparison to the other seasons (Figure 4) indicates

a strong freshwater influence that could be linked to significant freshwater release at the DPFD and the spring MR floods in 2010 and 2011, respectively. During the high flow conditions, the MR plume reversal and the plume water intrusion through the bay entrance into the lower bay previously reported in this region [26,30] were also observed in this study, as indicated by the relatively fresher water in the lower bay (Figure 4a, dashed ellipse) following the MR flood conditions in 2011. High a_g355 and relatively lower salinity at stations representing the measurements acquired on 1 June 2010 (Figure 4a, solid ellipse) corresponds to the period when a significant amount of the MR water was released through the DPFD during the high MR flow condition in 2010. Spectral slope values at these same stations (Figure 5a, solid ellipse) showed an increasing trend from the upper to central and lower bay sections indicating increasing effects of photo-oxidation in the lower bay. The effect of the fresher MR water was observed at all marine end members in April and May (2011) when the river experienced a severe flood event (Figures 4a and 5a, dashed ellipse). This effect is also observed in the satellite-derived CDOM distribution map and is examined in a later section.

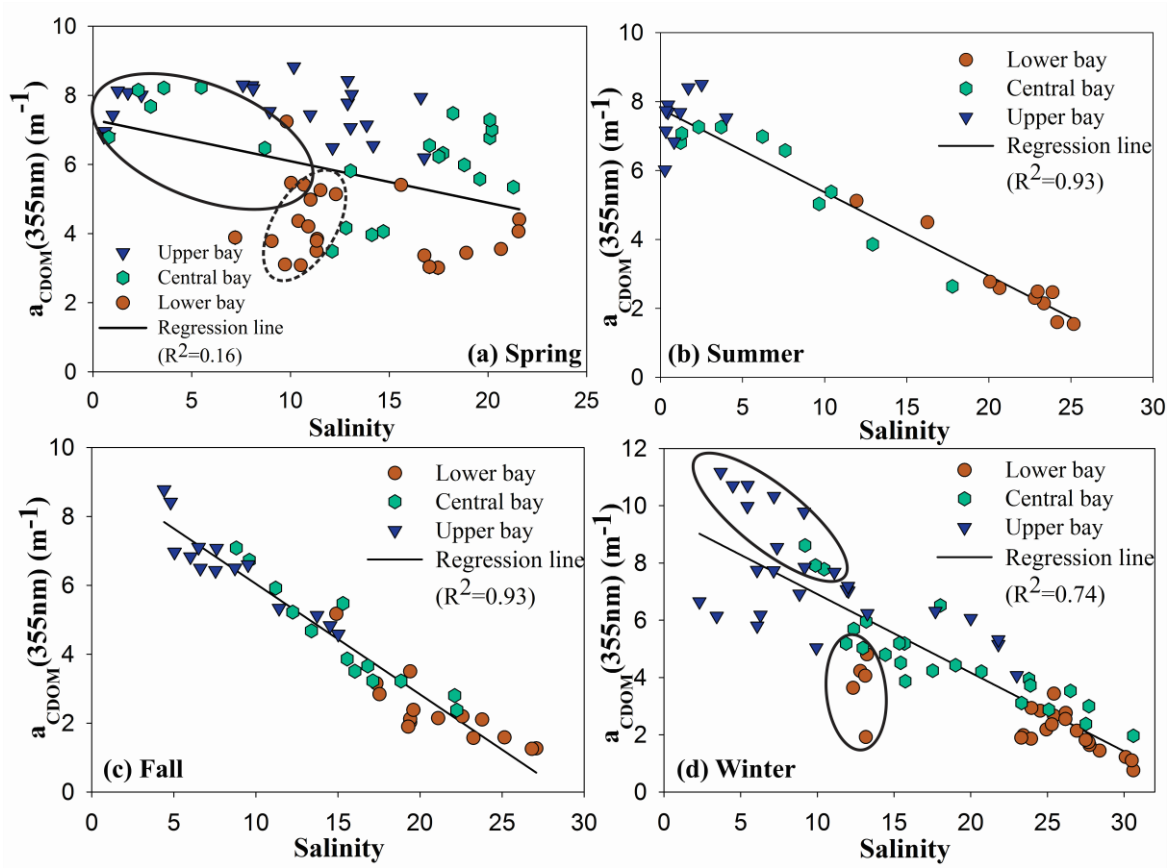

Figure 4. CDOM absorption coefficient (355nm) *vs.* salinity in (**a**) spring (the solid ellipse encloses measurements on 1 June 2010 associated with freshwater release at DPFD; the dashed ellipse encloses measurements at the marine stations on 6 April and 24 May 2011 associated with MR flood water), (**b**) summer, (**c**) fall, and (**d**) winter (solid ellipses correspond to measurements in Barataria Bay on 23 February 2010 associated with a high-pressure system (e.g., cold front)).

In the summer, a_g355 was more variable near the freshwater end members, whereas it followed a conservative mixing line (R^2 = 0.93) in the lower Barataria Bay (Figure 4b). This variability could be

attributed to varying amounts of precipitation and associated run-off in the upper Barataria Basin [25]. The spectral slope increased towards the marine environment during the summer, suggesting increased photo-oxidation of waters in the lower bay (Figure 4b). In the fall, a_g355-salinity showed a similar trend as observed in the summer (Figure 4c); however, $S_{275–295}$ was highly variable and increased towards the lower bay. The higher values of $S_{275–295}$ near the freshwater stations could be due to the increased residence time as the bay lacked potential CDOM sources such as mixing by strong winds, and significant freshwater supply through the DPFD and numerous channels during the low flow conditions (Figure 5c).

In the winter, the CDOM absorption coefficient was highly variable in the upper bay, and its variability reduced towards the marine stations (Figure 4d). A few freshwater stations experienced relatively higher a_g355 (> 10 m^{-1}) (Figure 4d). CDOM-rich freshwater was also observed in the central and even in the lower bay, despite the low flow condition (Figure 4d, solid ellipses). Relatively low $S_{275–295}$ at the same locations most likely indicated the supply of fresh CDOM in winter. These stations represented the measurement obtained on 23 February 2010 when the high-pressure system was passing over the bay. Strong winds associated with this system could have potentially mixed the shallow water column and released the CDOM trapped in sediments [10,56,57]. Furthermore, the lower salinities at the marine end member stations indicated the influence of strong wind forcing that could have introduced CDOM from other locations [27]. The observed anomalies ($S_{275–295}$ > 25 μm^{-1}) possibly indicated strong photo-bleaching near the marine end members in the winter [58–62] (Figure 5d).

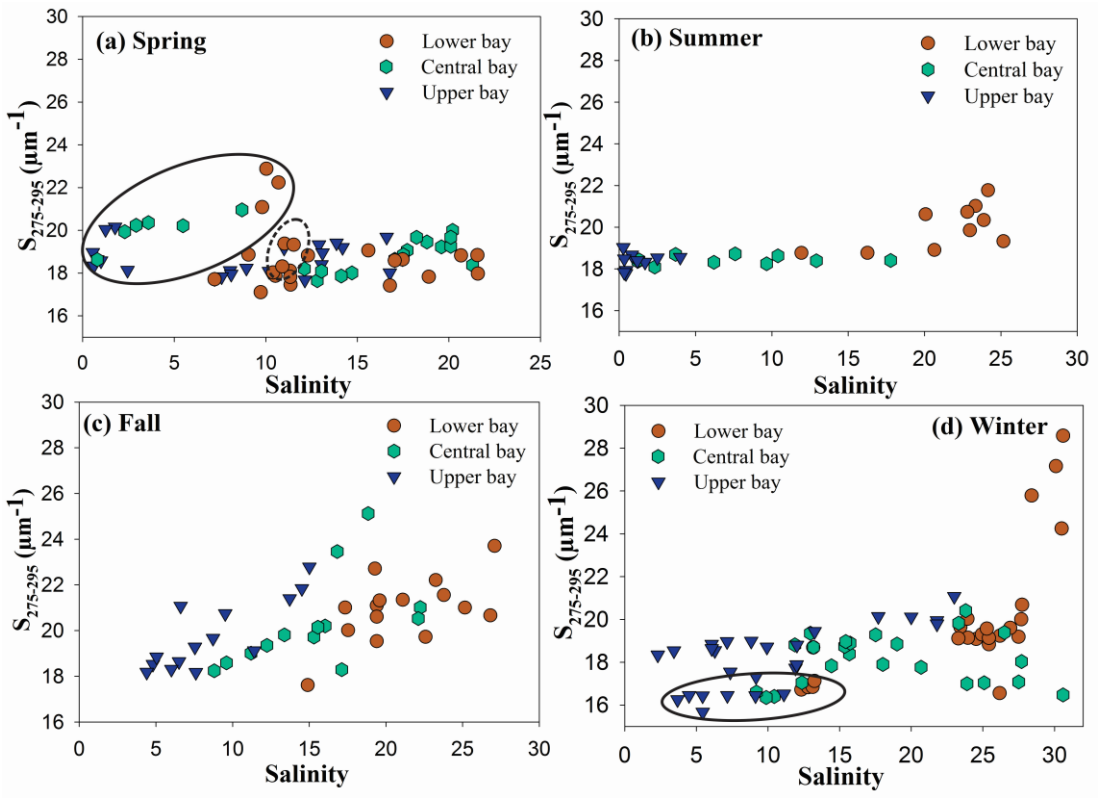

Figure 5. CDOM spectral slope *vs.* salinity relationship (**a**) spring, (**b**) summer, (**c**) fall, and (**d**) winter (the solid ellipse encloses similar measurements described in Figure 4).

3.2.3. Inter-Comparison of CDOM Variability during the DPFD Opening, the High MR Flow Condition, and the Passage of the High-Pressure System in 2010

Three major events during the study period appeared to strongly alter the CDOM abundance in Barataria Bay and their roles in the variability of a_g355 are examined in more detail. The months were divided into three groups based on the influence of their respective event, such as the MR high flow condition (MR = April and May), high-pressure systems (HP = November and February) and the DPFD opening (DPFD = June and August). Modeling studies in Barataria Bay indicated that freshwater influences the bay within 15–20 days after the diversion release at the DPFD [22,25]; therefore, the effects of DPFD opening were considered with a lag of 20 days (in June and August) from the observed peak discharge at the DPFD (in May and July), respectively. The mean a_g355 was 3.88 ± 1.33 m^{-1} and 7.52 ± 0.65 m^{-1} in the lower and upper bays, respectively, during the event of significant freshwater release at the DPFD. These values were not significantly different (two-sided t-test: $p = 0.5820$ and $p = 0.8460$) from the mean a_g355 during high flow condition in the MR, indicating the influence of MR water throughout the bay during high flow conditions and in the absence of significant freshwater release at the DPFD. In winter, the mean a_g355 was significantly higher (9.07 ± 1.49 m^{-1}; t-test: $p < 0.05$) than the DPFD in the upper bay suggesting, that the strong winds can be more influential than the freshwater release, especially during the passage of intense high-pressure systems, as the one that affected the measurements in February 2010. Although mean a_g355 was relatively lower, the effect of the high-pressure system was not significantly different in the lower bay relative to the freshwater diversion and high flow conditions.

3.2.4. A Tree-Based Analysis of the CDOM Absorption Coefficient

The marine end member (Station 1) is located just outside the bay with relatively similar proximity to both the DPFD and the MR south pass. Therefore, it is considered as the ideal location to examine the relative importance of various factors, such as wind speed, wind direction, Mississippi River discharge at Belle Chasse and discharge at DPFD on CDOM variability. Figure 6a illustrates a pruned decision tree for a_g355 at Station 1. A root node (Node-1) is a starting point that includes all data (N = 14 months, data = 100%). The MR discharge at Belle Chasse was the most important factor strongly affecting the variability of a_g355 at station-1. The mean a_g355 for this group was 2.7 m^{-1}. The observations were split (threshold value = 20,000 $m^3 \cdot s^{-1}$) further based on the high and low flow conditions. The high flow condition occurred during four months in the spring of 2010 and 2011. These months include both the freshwater release at DPFD and the MR flood condition when relatively higher a_g355 (Node-3, mean = 4 m^{-1}, data = 29%) were observed at Station 1.

During the high flow conditions, discharge at the DPFD was another important factor that affected a_g355 near the marine end members. A significant amount of freshwater (>140 $m^3 \cdot s^{-1}$) was released from DPFD during the high flow condition (node = 7, mean = 5 m^{-1}, data = ~7%), which could have resulted in the higher mean a_g355 at this node relative to Node-3. This suggests the combined influence of two freshwater sources at the marine end members and likely represents the month of May in 2010 when a significant amount of freshwater was released into Barataria Bay to flush crude oil out of the bay during the high MR flow condition (Figure 2, Panels 1 and 2). Low discharge at DPFD had no effect on a_g355

at the marine station (node = 6, N = 3, data = ~21%). This node also showed that there was no linkage between high river flow conditions in the MR and the freshwater diversion at DPFD, since low discharge was reported at DPFD for three months, despite high river flow in the MR. During the low MR flow conditions, wind speed became another important factor in the lower Barataria Bay. The low flow condition (<20,000 $m^3 \cdot s^{-1}$) was evident for 71% of measurements with a mean a_g355 of 2.2 m^{-1} (Node-2). Node-2 represents months in the summer, fall and winter seasons (the MR discharge, Figure 2; and a_g355, Table 3). Node-2 is further linked into two groups, Node-4 (mean = 1.9 m^{-1}, N = 6, data = ~43%) and Node-5 (mean = 2.8 m^{-1}, N = 4, data = ~29%). At Node-5, elevated mean a_g355 likely suggests the influence of strong winds at Station 1. An unpruned tree demonstrated the dominance of northerly winds at Node-5, suggesting that the high-pressure systems were responsible for approximately an ~21% increase in mean a_g355 during 2010 and 2011 (Figure 6b). In contrast, low wind speeds were responsible for an ~14% decrease in mean a_g355 during six months (node = 4, mean = 1.9 m^{-1}, data = ~43%) and likely to represent the months in summer and fall. The unpruned tree showed the dominance of southerly winds during this period and that could be another reason of reduced a_g355 due to increased residence time, dilution by marine water, and reduced supply of CDOM. In summary, high river flow conditions, high-pressure systems and low-pressure systems were controlling a_g355 by approximately 28%, 29% and 43%, respectively at station-1 in 2010 and 2011. The Mississippi River flow was the most important factor controlling a_g355 variability followed by discharge at DPFD and wind speed at Station 1.

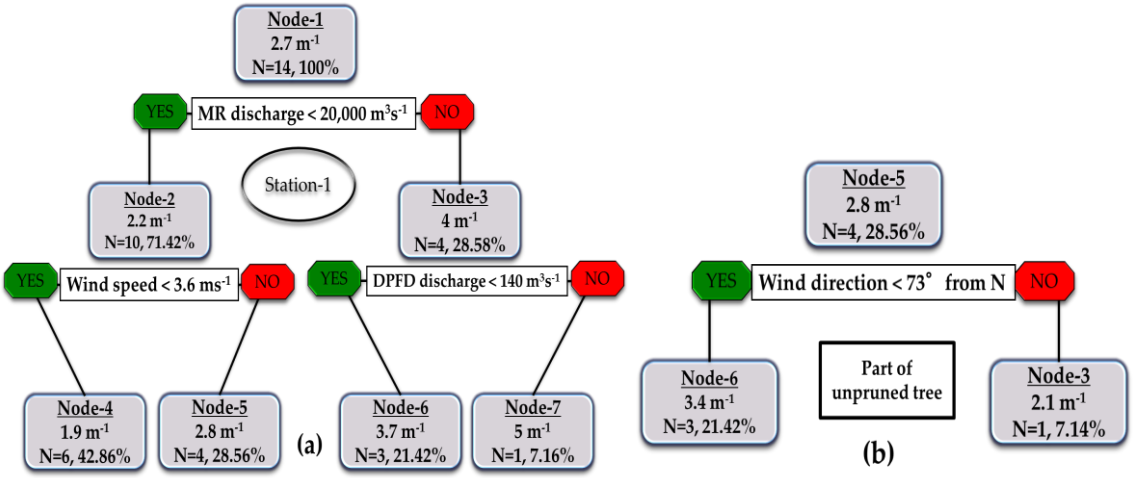

Figure 6. (a) Decision tree for a_g355 at Station 1. The groups are represented by mean, number of samples (months) and percentage (%) of total measurements. **(b)** Part of the unpruned tree shows the influence of northerly winds at Node-5.

Thus, various meteorological and hydrological factors have been shown to influence CDOM optical properties in the different sections of the bay during various seasons (e.g., the MR water in lower bay in spring, and CDOM-rich freshwater, wind speed and precipitation/run-off in the upper bay in spring, summer and winter, respectively). In 2010, CDOM characteristics changed greatly due to a series of meteorological and hydrological events in Barataria Bay and the effects of high-pressure systems were the strongest among all, especially in the upper bay. The tree-based statistical analysis indicated that the majority of CDOM variation was linked to the MR high flow condition followed by the freshwater discharge at DPFD and wind speed at the marine end member.

3.3. Satellite Assessment of CDOM Variability in the Barataria Bay

3.3.1. Band Selection for the Empirical Algorithm

The reflectance spectrum is generally characterized by low reflectance at the blue wavelength and relatively high reflectance at the green and red wavelengths in coastal waters [44]. A general exponential increase in CDOM absorption towards the shorter wavelengths suggests greater variations in the green and blue wavebands corresponding to the alteration in CDOM abundance. Hence, the blue (Band-1, 0.45–0.52 μm) and green (Band-2, 0.52–0.60 μm) spectral regions can be the most suitable spectral regions for capturing variation in CDOM abundance in terms of a statistical relationship between a_g355 and the satellite observed surface reflectance. Elevated concentrations of phytoplankton and non-algal particulate matter have significant contribution to light attenuation in the blue region in the estuarine environment. Additionally, the strong influence of CDOM reduces blue light, resulting in a weak water-leaving signal in the blue region that is often close to zero or below the detection level. Hence, the errors in atmospheric correction are likely to be the largest in the blue part of the spectrum [63]. Furthermore, sky light also contributes strongly to blue wavelengths during clear sky conditions. Therefore, despite the large variation in CDOM absorption in the blue part of spectrum, Band-2 was considered over Band-1 for this analysis. In the red region (Band-3, 0.63–0.69 μm), variation in water-leaving radiance is mainly affected by backscattering with little influence of CDOM. Many studies have demonstrated the successful use of the green (Band-2) and red (Band-3) regions to measure water quality in freshwater environments [34,35,37,63]. Landsat Band-3 was utilized as a reference to develop an empirical algorithm for the CDOM absorption coefficient in this study.

Field collected a_g355 values were used as the dependent variable in linear and non-linear regression against various combinations of Bands 2, 3, and 4; a combination of Band 2 and Band 3 using Landsat5- TM imagery (Table 1) showed the highest correlation ($R^2 = 0.74$, range = 1.25–8.54 m^{-1} ; N = 50, $p < 0.0001$) on the training data set,

$$a_g355 = 6.68\ (B2/B3)^{-3.12} \quad (4)$$

This relationship was evaluated on the test data set (range = 1.10–8.43 m^{-1}; N = 28) and utilized to generate CDOM maps for further analysis.

3.3.2. The CDOM Empirical Algorithm for the Landsat Sensor

A non-linear power law relationship between the CDOM absorption coefficient and Landsat-5 TM band ratio (B2/B3) is illustrated in Figure 7a ($R^2 = 0.74$, N = 50, $p < 0.0001$). This relationship has been developed using the images acquired during the spring, fall and winter seasons, while it has been validated on two images from the winter and spring. The validation yielded $R^2 = 0.76$ (N = 28, $p < 0.0001$), RMSE = 1.16 m^{-1}, and bias = 2.88% (Figure 7b). The upper bay showed the highest RMSE (1.28 m^{-1}) compared to the lower bay (0.80 m^{-1}) suggesting the greater variability in a_g355 during the time of image acquisition. Although the algorithm validation results indicated relatively acceptable RMSE (= 1.16 m^{-1}, range = 1.10–8.43 m^{-1}) for the estuarine environment, several factors may have contributed to the difference (absolute bias) in the matchup comparison of the observed and estimated a_g355. In winter, strong wind associated with the cold fronts can mix the water column and release

CDOM trapped in the bottom sediments [33,64,65]. Furthermore, the narrow width and the shallow depths of the upper bay make it susceptible to relatively strong mixing of the water column by winds and tidal currents in contrast to the relatively wide and deep lower part of the bay [66]. Therefore, variability in the water characteristics of the upper bay could have contributed to the more significant RMSE in the matchup comparison. In contrast, the observed small RMSE in the lower bay could be due to relatively more stable characteristics, except during periods of strong winds [59]. The time difference between image acquisition and *in-situ* measurements can also cause large errors in the performance of an algorithm. The empirical algorithm presented in this study utilized clear sky images acquired within ±5 days of *in-situ* measurement. CDOM abundance is likely to be quite variable, as Barataria Bay is governed by different meteorological and hydrological factors throughout the year. Although it is difficult to get a satellite image within a few hours of *in-situ* measurements due to the coarse temporal resolution of Landsat and possibly unfavorable weather conditions, the images acquired on the same day of measurements are likely to improve the CDOM estimation. The discrepancy in the matchup analysis could also have occurred due to the effects of high concentrations of particulate matter on the water leaving radiance. Since Landsat has a wide spectral band (bandwidth = 0.08 µm compared to 0.01 µm of the MODIS green band), light attenuation by particulate matter is likely to introduce an error in a_g355 estimation, especially in the shallow and turbid bays. The red region (Band-3, 0.63–0.69 µm) of Landsat-5 TM includes the phytoplankton absorption peak, which could degrade the algorithm performance, especially during the periods of phytoplankton blooms. Furthermore, the contributions of sky light and whitecaps cannot be ignored on the surface reflectance and therefore, on the algorithm performance. In spite of numerous limitations, the CDOM algorithm and its validation indicated the possibility of using Landsat imagery to monitor CDOM in shallow bays.

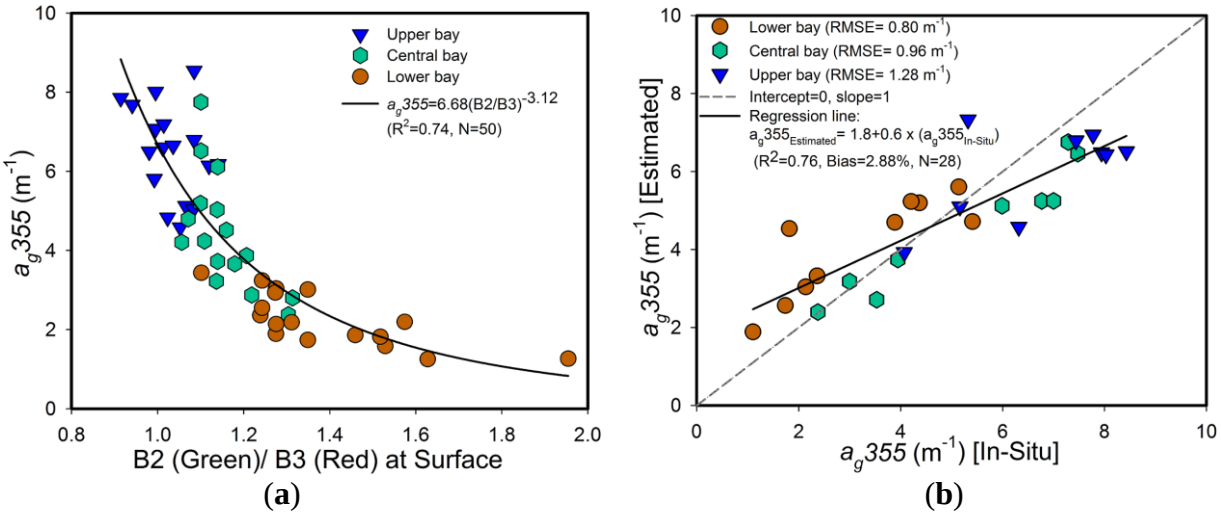

Figure 7. (**a**) Power law relationship between the CDOM absorption coefficient and the Landsat band ratio (Green/Red). The a_g355 band ratio algorithm: $a_g355 = 6.68 \times (B2/B3)^{-3.12}$ ($R^2 = 0.74$, N = 50). (**b**) Validation of a band ratio algorithm ($R^2 = 0.76$, N = 28).

3.3.3. Hydrological and Meteorological Influences—Landsat Satellite Assessment

Four Landsat TM images obtained during the study period were converted to the CDOM maps to study the effect of different conditions (physical, meteorological and hydrological; Figure 8) on CDOM variability in Barataria Bay during the period of image acquisition. Barataria Bay experienced a high pressure system on 25 February 2010, and the associated impact of the frontal passage on CDOM absorption is illustrated in Figure 9a. The Mississippi River discharge was high (~25,000 $m^3 \cdot s^{-1}$), while discharge at DPFD was low (~30 $m^3 \cdot s^{-1}$). However, the bay experienced strong winds from the north, resulting in high a_g355 in the upper bay towards Little Lake despite low fresh water flow at DPFD (daily mean salinity = ~5). Winds likely pushed bay water to the shelf through the tidal channels between barrier islands and that might have reduced salinity at Station 1 (daily mean salinity = ~14) due to the fresh and marine water mixing (Figure 8).

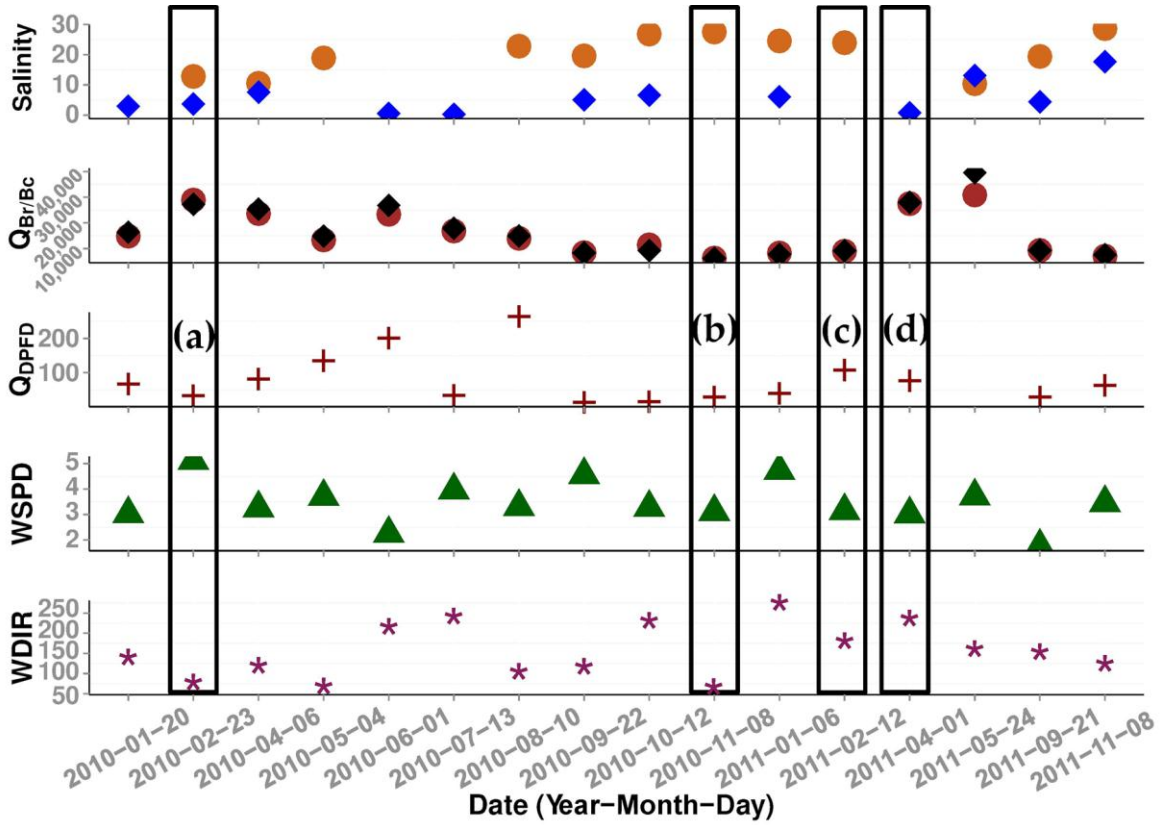

Figure 8. Time-series of salinity (Station 1: dots; Station 15: diamonds), the Mississippi river discharge at Baton Rouge (Q_{BR}: diamonds) and Belle Chasse (Q_{BC}: dots) (m^3/s), discharge at Davis Pond Freshwater Diversion (Q_{DPFD}) ($m^3 \cdot s^{-1}$), wind speed (m/s) and wind direction (degrees from north) corresponding to monthly-observed a_g355 (m^{-1}) in Barataria Bay in 2010 and 2011. The boxes (**a**–**d**) represent the meteorological and hydrological conditions corresponding to the CDOM maps illustrated in Figure 9.

CDOM imagery of 8 November 2010 (Figure 9b) shows the influence of a relatively weak high-pressure system. Relatively high a_g355 (>7 m^{-1}) is evident to the north of the bay in Little Lake. The plume-like features of relatively high a_g355 are seen extending into the shelf waters through the tidal inlets near the mouth of the bay. The mean daily salinity of ~30 was observed at Station 1, suggesting

no direct effect of the MR discharge (~7000 $m^3 \cdot s^{-1}$ at Belle Chasse) and the discharge at the DPFD (~28 $m^3 \cdot s^{-1}$). However, the bay experienced intermediate northeasterly winds (daily mean = ~3 m/s) that could have contributed to the higher CDOM bay waters being transported into the shelf (Figure 8).

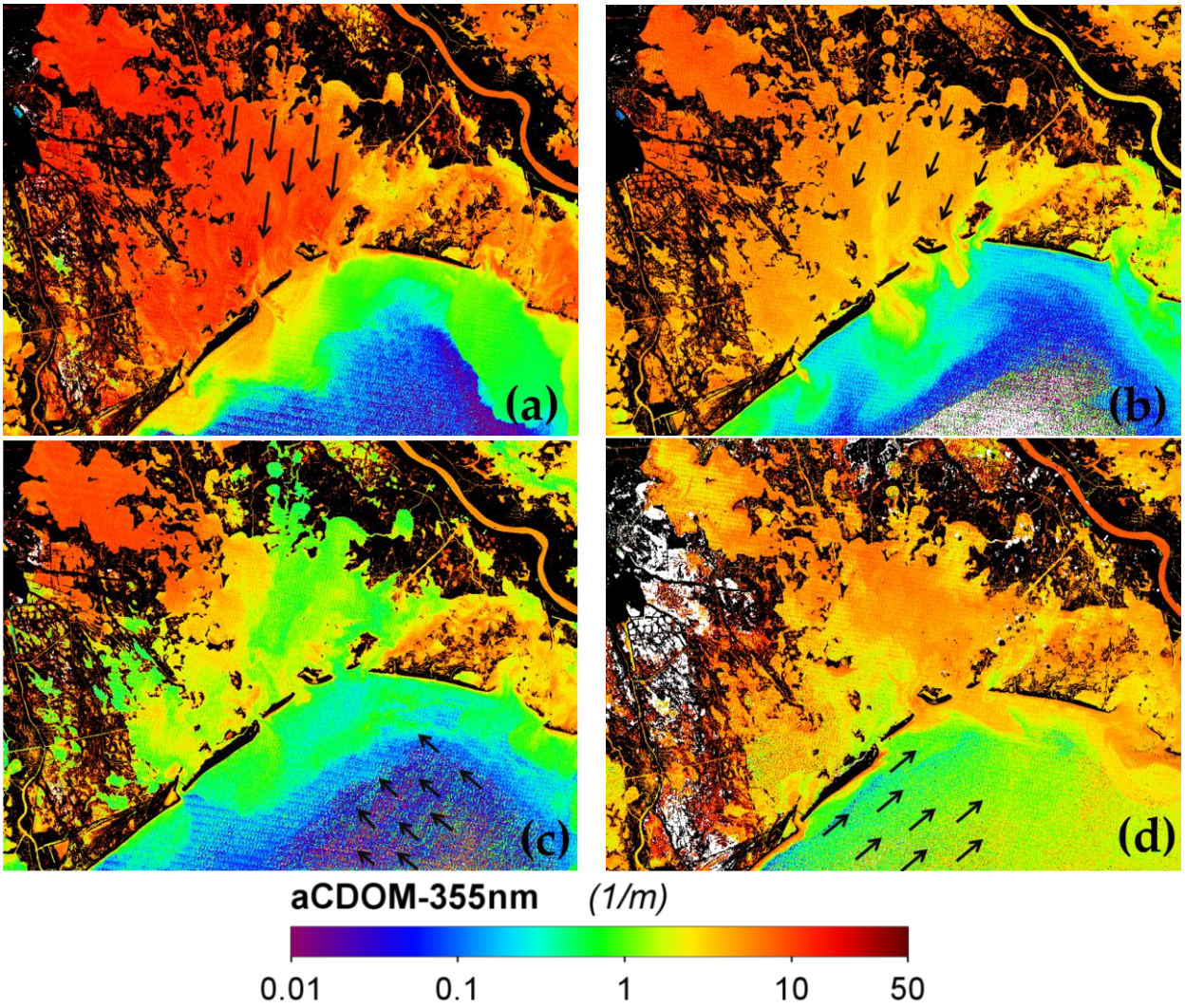

Figure 9. Landsat-5 TM-derived CDOM imagery of the Barataria Bay and Louisiana coastal waters obtained using Equation 4 during (**a**) a strong frontal system (25 February 2010), (**b**) a weak high-pressure system (8 November 2010), (**c**) elevated freshwater release at DPFD (12 February 2011) and (**d**) high MR flow condition (1 April 2011) (black arrows represent approximate daily mean wind direction, with longer arrows indicating stronger winds and *vice versa*).

The third case demonstrates the distribution of a_g355 on 12 February 2011 (Figure 9c). Although, the MR experienced low flow conditions (< 15,000 $m^3 \cdot s^{-1}$), the discharge at DPFD was moderate (> 100 $m^3 \cdot s^{-1}$). High a_g355 observed in the upper bay can be associated with the moderate fresh water flow at the DPFD. Weak winds from the south/southeast direction were likely to push marine water towards the bay that could have contributed to high salinity (~30) at Station 1 despite the moderate freshwater discharge at the DPFD (Figure 4).

Figure 9d shows the CDOM distribution in the high river flow condition (1 April 2011), during which Barataria Bay and the surrounding areas had experienced one of the most damaging flood events in U.S. history. The Mississippi River discharge was reported to be ~28,500 $m^3 \cdot s^{-1}$ at Belle Chasse, while discharge at the DPFD was moderately high (~70 $m^3 \cdot s^{-1}$) (Figure 8). Interestingly, the map revealed high values of a_g355 in the Mississippi River that could be associated with the floodwaters. Relatively high a_g355 in shelf water was likely due to the influence of the Mississippi River plume in the Louisiana Bight. The presence of westerly/southwesterly winds (daily mean = ~3 $m \cdot s^{-1}$) could also have supported the influence of CDOM-rich plume water towards the mouth of the bay [26,30]. The eastern part of the bay also experienced higher a_g355 values likely due to the freshwater input from the DPFD and the numerous channels in the north and east (e.g., West Pointe à la Hache siphon diversion) regions of the bay during the high flow conditions of the MR [25].

It is worth noting that the algorithm failure in the clear offshore shelf waters (e.g., Figure 9b) could be attributed to the absence of particulate load and, thus, low reflectance of the reference band (B3) that resulted in close to null a_g355 values. However, elevated water turbidity along the coast, where the algorithm shows relatively detectable a_g355, indicates that the algorithm works well in the more turbid environment (Figure 9d). This section showed that the Landsat5- TM-derived CDOM empirical relationship successfully captured the major details of CDOM distribution and seasonal influence in Barataria Bay, although some uncertainty exists in the algorithm performance. The empirical relationship can be further improved by considering a larger number of images, a smaller time difference between the *in-situ* and satellite observations, the use of different Landsat sensors (e.g., a combination of Landsat-7 ETM+ and Landsat-8 OLI) and suitable corrections for particulate matter, sky light and whitecaps.

4. Conclusions

Barataria Bay is an optically complex transition zone that is influenced by various meteorological and hydrological phenomena throughout the year. The effects of meteorological and hydrological factors such as wind speed, freshwater diversions, and river discharge on spatial and seasonal variability in the CDOM absorption coefficient (a_g355) in Barataria Bay were investigated in detail. CDOM abundance was the highest in the spring among all seasons. The bay was characterized by a general trend of low a_g355 and higher variability near the marine end members, as well as high a_g355 with the lower variability towards the freshwater end members. Salinity and $S_{275–295}$ were greatly variable in the lower bay in all seasons, whereas the lowest variability was observed in the upper bay, except during the summer. The mean surface temperature together with salinity suggested the influence of the MR water from the south in the lower bay in the spring.

The bay experienced three major events, the high MR flow and a large amount of freshwater diversion in the spring, as well as the passage of a cold front in the winter in 2010. Relatively higher a_g355 values were observed during the opening of the DPFD. However, large spectral slopes in the central and upper bays indicated the degradation of CDOM, possibly due to the influence of the MR plume that could have increased the residence time by entrapping the bay water. The passage of a high- pressure system contributed to the increase in a_g355 and the decrease in $S_{275–295}$, despite the lack of hydrological inputs of CDOM and it showed that the meteorological factors were as important as the hydrological factors to

control CDOM abundance, especially in the upper and central Barataria Bay. The inter-comparison analysis of CDOM variability in 2010 showed that the MR was a major factor in controlling a_g355 variability; thus, CDOM abundance in the lower bay during the high flow conditions, and periods of strong winds were capable of elevating the CDOM abundance even higher than during the freshwater diversion in the upper bay. The tree-based statistical analysis showed the influence of high river flow conditions and high- and low-pressure systems that appeared to control a_g355 by ~28%, 29% and 43% of the time duration over the study period at the marine end members. In conclusion, the occurrences of the hydrological and meteorological events can potentially cause anomalous a_g355 compared to the "normal condition" in Barataria Bay. The performance of the CDOM algorithm can be greatly affected by these events and therefore it is necessary to capture the effects of hydrological and meteorological factors in the algorithm development.

We hypothesized that the bay should mimic terrestrial systems since terrestrially-derived DOM is a major source of CDOM in the bay and it could be monitored using Landsat imagery. For Landsat, Band 2/Band 3 values were obtained from six clear sky images and correlated with a_g355 to construct a band ratio empirical algorithm. A validation of the empirical logarithmic relationship showed high correlation ($R^2 = 0.76$). A comparison of *in-situ* and satellite-derived a_g355 revealed that the upper bay showed the largest RMSE followed by the central and the lower bay. Several factors could have contributed to the discrepancy between the observed and predicted a_g355, such as time differences between image acquisition and *in-situ* observation, a strong influence of seasonally-dependent hydrological and meteorological factors, limited temporal and spatial resolution of the data, and the optical interference of particulate matter, sky light and whitecaps on the water leaving radiance.

Although some uncertainty exists in the Landsat5- TM derived CDOM empirical relationship, it has successfully captured major details of CDOM distribution and seasonal influence in Barataria Bay. The empirical relationship can be further improved by considering a larger number of images, a smaller time difference between the *in-situ* and satellite observations, the use of different Landsat sensors (e.g., a combination of Landsat-7 ETM+ and Landsat-8 OLI) and suitable correction for particulate matter, sky light and whitecaps. Although the proposed empirical algorithm has been shown to work well in Barataria Bay, it could be subject to change in the band combination, coefficients or regression function if it is used in other coastal regions; nonetheless, the promising performance of the empirical CDOM Landsat algorithm supports the use of Landsat data in carbon cycle studies in coastal aquatic environments.

Acknowledgments

The authors are grateful to Dr. Eugene Turner from Department of Oceanography & Coastal Sciences, Louisiana State University for the water samples used in this study. The authors acknowledge partial support provided by a NASA grant (No. NNX14A043G).

Author Contributions

The authors contributed equally to this work.

Conflicts of Interest

The authors declare no conflict of interest.

References

1. Kirk, J.T.O. *Light and Photosynthesis in Aquatic Ecosystems*; Cambridge University Press: Cambridge, UK, 1994.
2. Blough, N.V.; Green, S.A. Spectroscopic characterization and remote sensing of non-living organic matter. In *The Role of Non-living Organic Matter in the Earth's Carbon Cycle*; Zepp, R.G., Sonntag, C., Eds.; John Wiley Sons Ltd: Hoboken, NJ, USA, 1995; pp. 23–45.
3. Blough, N.V.; Del Vecchio, R. Chromophoric DOM in the coastal environment. In *Biogeochemistry of Marine Dissolved Organic Matter*; Hansell D., Carlson C.A., Eds.; Academic Press, 2002; pp. 509–546.
4. Bricaud, A.; Morel, A.; Prieur, L. Absorption by dissolved organic matter of the Sea (yellow substance) in the UV and visible domains. *Limnol. Oceanogr.* **1981**, *26*, 43–53.
5. Bianchi, T.S. The role of terrestrially derived organic carbon in the coastal ocean: A changing paradigm and the priming effect. *Proc. Natl. Acad. Sci.* **2011**, *108*, 19473–19481.
6. Coble, P.G.; Del Castillo, C.E.; Avril, B. Distribution and optical properties of CDOM in the Arabian Sea during the 1995 Southwest Monsoon. *Deep Sea Research Part II: Topical Stud. Oceanogr.* **1998**, *45*, 2195–2223.
7. Del Castillo, C.E.; Gilbes, F.; Coble, P.G.; Müller-Karger, F.E. On the dispersal of riverine colored dissolved organic matter over the West Florida Shelf. *Limnol. Oceanogr.* **2000**, *45*, 1425–1432.
8. Morel, A.; Prieur, L. Analysis of variations in ocean color. *Limnol. Oceanogr.* **1977**, *22*, 709–722.
9. Steinberg, D.K.; Nelson, N.B.; Carlson, C.A.; Prusak, A.C. Production of Chromophoric Dissolved Organic Matter (CDOM) in the open ocean by zooplankton and the colonial cyanobacterium *Trichodesmium Spp*. *Mar. Ecol. Prog. Ser.* **2004**, *267*, 45–56.
10. D'Sa, E.J.; Ko, D.S. Short-term influences on suspended particulate matter distribution in the northern Gulf of Mexico: Satellite and model observations. *Sensors* **2008**, *8*, 4249–4264.
11. D'Sa, E.J.; Miller, R.L.; Del Castillo, C. Bio-optical properties and ocean color algorithms for coastal waters influenced by the Mississippi River during a cold front. *Appl. Opt.* **2006**, *45*, 7410–7428.
12. Siegel, D.A.; Maritorena, S.; Nelson, N.B.; Hansell, D.A.; Lorenzi-Kayser, M. Global distribution and dynamics of colored dissolved and detrital organic materials. *J. Geophys. Res. Ocean. (1978–2012)* **2002**, *107*, doi:10.1029/2001JC000965.
13. Bianchi, T.S.; Pennock, J.R.; Twilley, R.R. *Biogeochemistry of Gulf of Mexico Estuaries*. John Wiley Sons: Hoboken, NJ, 1999.
14. Rabalais, N.N.; Turner, R.E.; Wiseman, W.J., Jr. Gulf of Mexico hypoxia, AKA "the dead zone". *Ann. Rev. Ecol. Syst.* **2002**, *33*, 235–263.
15. Rabalais, N.N.; Turner, R.E.; Wiseman, W.J. Hypoxia in the Gulf of Mexico. *J. Environ. Qual.* **2001**, *30*, 320–329.
16. Sklar, F.H.; Turner, R.E. Characteristics of Phytoplankton Production off Barataria Bay in an Area Influenced by the Mississippi River. Available online: http://agris.fao.org/agris-search/search.do?recordID=US19830857423 (accessed on 27 July 2015).

17. Britsch, L.D.; Kemp Iii, E.B. *Land Loss Rates: Mississippi River Deltaic Plain*; Defense Technical Information Center: Fort Belvoir, VA, USA, 1990.
18. Conner, W.H.; Day Jr, J.W. *The Ecology of Barataria Basin, Louisiana: An Estuarine Profile*; Louisiana State University;. Center for Wetland Resources: Baton Rouge, LA, USA, 1987.
19. Day, J.W.; Boesch, D.F.; Clairain, E.J.; Kemp, G.P.; Laska, S.B.; Mitsch, W.J.; Orth, K.; Mashriqui, H.; Reed, D.J.; Shabman, L. Restoration of the Mississippi Delta: Lessons from hurricanes Katrina and Rita. *Science* **2007**, *315*, 1679–1684.
20. Penland, S.; Connor Jr, P.F.; Beall, A.; Fearnley, S.; Williams, S.J. Changes in Louisiana's shoreline: 1855–2002. *J. Coast. Res.* **2005**, *44*, 7–39.
21. Bianchi, T.S.; Cook, R.L.; Perdue, E.M.; Kolic, P.E.; Green, N.; Zhang, Y.; Smith, R.W.; Kolker, A.S.; Ameen, A.; King, G. Impacts of diverted freshwater on dissolved organic matter and microbial communities in Barataria Bay, Louisiana, USA. *Mar. Environ. Res.* **2011**, *72*, 248–257.
22. Inoue, M.; Park, D.; Justic, D.; Wiseman, W.J. A high-resolution integrated hydrology-hydrodynamic model of the Barataria Basin system. *Environ. Model. Softw.* **2008**, *23*, 1122–1132.
23. Booth, J.G.; Miller, R.L.; McKee, B.A.; Leathers, R.A. Wind-induced bottom sediment resuspension in a microtidal coastal environment. *Continental Shelf Res.* **2000**, *20*, 785–806.
24. Reed, D.J. Patterns of sediment deposition in subsiding coastal salt marshes, Terrebonne Bay, Louisiana: The role of winter storms. *Estuaries* **1989**, *12*, 222–227.
25. Park, D. Hydrodynamics and freshwater diversion within Barataria Basin. Ph.D. Thesis, Louisiana State University, Baton Rouge, LA, USA, 2002.
26. Hitchcock, G.L.; Chen, R.F.; Gardner, G.B.; Wiseman, W.J. A Lagrangian view of fluorescent chromophoric dissolved organic matter distributions in the Mississippi River plume. *Mar. Chem.* **2004**, *89*, 225–239.
27. Singh, S.; D'Sa, E.; Swenson, E. Seasonal variability in CDOM absorption and fluorescence properties in the Barataria Basin, Louisiana, USA. *J. Environ. Sci.* **2010**, *22*, 1481–1490.
28. D'Sa, E.J.; DiMarco, S.F. Seasonal variability and controls on chromophoric dissolved organic matter in a large river-dominated coastal margin. *Limnol. Oceanogr.* **2009**, *54*, 2233–2242.
29. Boss, E.; Pegau, W.S.; Zaneveld, J.R.V.; Barnard, A.H. Spatial and temporal variability of absorption by dissolved material at a continental shelf. *J. Geophys. Res. Ocean.* **2001**, *106*, 9499–9507.
30. Li, C.; White, J.R.; Chen, C.; Lin, H.; Weeks, E.; Galvan, K.; Bargu, S. Summertime tidal flushing of Barataria Bay: Transports of water and suspended sediments. *J. Geophys. Res. Ocean.* **2011**, *116*, doi:10.1029/2010JC006566.
31. D'Sa, E.; Hu, C.; Muller-Karger, F.; Carder, K. Estimation of colored dissolved organic matter and salinity fields in Case 2 waters using SeaWIFS: Examples from Florida Bay and Florida Shelf. *J. Earth Syst. Sci.* **2002**, *111*, 197–207.
32. Del Castillo, C.E.; Miller, R.L. On the use of ocean color remote sensing to measure the transport of dissolved organic carbon by the Mississippi River plume. *Remote Sens. Environ.* **2008**, *112*, 836–844.
33. Tehrani, N.C.; D'Sa, E.J.; Osburn, C.L.; Bianchi, T.S.; Schaeffer, B.A. Chromophoric dissolved organic matter and dissolved organic carbon from sea-viewing wide field-of-view sensor (SeaWIFS), Moderate Resolution Imaging Spectroradiometer (MODIS) and MERIS sensors: Case study for the northern Gulf of Mexico. *Remote Sens.* **2013**, *5*, 1439–1464.

34. Brezonik, P.; Menken, K.D.; Bauer, M. Landsat-based remote sensing of lake water quality characteristics, including chlorophyll and Colored Dissolved Organic Matter (CDOM). *Lake Reserv. Manag.* **2005**, *21*, 373–382.
35. Ficek, D.; Zapadka, T.; Dera, J. Remote sensing reflectance of Pomeranian lakes and the Baltic. *Oceanologia* **2011**, *53*, 959–970.
36. Griffin, C.G.; Frey, K.E.; Rogan, J.; Holmes, R.M. Spatial and interannual variability of dissolved organic matter in the Kolyma River, East Siberia, observed using satellite imagery. *J. Geophys. Res. Biogeosci.* **2011**, doi:10.1029/2010JG001634.
37. Kutser, T. The possibility of using the Landsat image archive for monitoring long time trends in coloured dissolved organic matter concentration in lake waters. *Remote Sens. Environ.* **2012**, *123*, 334–338.
38. Penland, S.; Roberts, H.; Williams, S.; Sallenger Jr, A.; Cahoon, D.R.; Davis, D.W.; Groat, C. Coastal land loss in Louisiana. **1990**, *40*, 685–699.
39. Swenson, E.M.; Turner, R.E. *Past, Present and Probable Future Salinity Variations in the Barataria Estuarine System*; Louisiana State University: Baton Rouge, LA, USA, 1998.
40. Green, S.A.; Blough, N.V. Optical absorption and fluorescence properties of chromophoric dissolved organic matter in natural waters. *Limnol. Oceanogr.* **1994**, *39*, 1903–1916.
41. Jerlov, N.G. *Marine Optics*; Elsevier: New York, NY, USA, 1976.
42. D'Sa, E.; Goes, J.; Gomes, H.; Mouw, C. Absorption and fluorescence properties of chromophoric dissolved organic matter of the eastern Bering Sea in the summer with special reference to the influence of a cold pool. *Biogeosciences* **2014**, *11*, 3225–3244.
43. Gordon H.; Wang M. Retrieval of water-leaving radiance and aerosol optical thickness over the oceans with SeaWiFS: a preliminary algorithm. *Appl. Opt.* **1994**, 33, 443–452.
44. Mobley, C.D. *Light and Water: Radiative Transfer in Natural Waters*. Academic Press: Waltham, MA, USA, 1994.
45. Breiman, L.; Friedman, J.; Stone, C.J.; Olshen, R.A. *Classification and Regression Trees*; CRC Press: Baton Rouge, LA, USA, 1984.
46. Podgorelec, V.; Kokol, P.; Stiglic, B.; Rozman, I. Decision trees: An overview and their use in medicine. *J. Med. Syst.* **2002**, *26*, 445–463.
47. Wu, J.; Olesnikova, A.; Song, C.-H.; Lee, W.D. The development and application of decision tree for agriculture data. In Proceedings of the Second International Symposium on Intelligent Information Technology and Security Informatics, Moscow, Russia, 23–25 January 2009; pp 16–20.
48. Gandomi, A.H.; Fridline, M.M.; Roke, D.A. Decision Tree Approach for Soil Liquefaction Assessment. Available online: http://www.hindawi.com/journals/tswj/2013/346285/ (accessed on 27 July 2015).
49. De'ath, G.; Fabricius, K.E. Classification and regression trees: A powerful yet simple technique for ecological data analysis. *Ecology* **2000**, *81*, 3178–3192.
50. Torgo, L. Inductive learning of tree-based regression models. *AI Commun.* **2000**, *13*, 137–138.
51. Schaffer, C. Selecting a classification method by cross-validation. *Mach. Learn.* **1993**, *13*, 135–143.
52. Das, A.; Justić, D.; Swenson, E. Modeling estuarine-shelf exchanges in a deltaic estuary: Implications for coastal carbon budgets and hypoxia. *Ecol. Model.* **2010**, *221*, 978–985.

53. Fichot, C.G.; Benner, R. The spectral slope coefficient of chromophoric dissolved organic matter ($S_{275–295}$) as a tracer of terrigenous dissolved organic carbon in river-influenced ocean margins. *Limnol. Oceanogr.* **2012**, *57*, 1453–1466.
54. Helms, J.R.; Stubbins, A.; Ritchie, J.D.; Minor, E.C.; Kieber, D.J.; Mopper, K. Absorption spectral slopes and slope ratios as indicators of molecular weight, source, and photobleaching of chromophoric dissolved organic matter. *Limnol. Oceanogr.* **2008**, *53*, 955–969.
55. Vodacek, A.; Blough, N.V.; DeGrandpre, M.D.; Nelson, R.K. Seasonal variation of CDOM and DOC in the middle Atlantic Bight: Terrestrial inputs and photooxidation. *Limnol. Oceanogr.* **1997**, *42*, 674–686.
56. Feng, Z.; Li, C. Cold-front-induced flushing of the Louisiana Bays. *J. Mar. Syst.* **2010**, *82*, 252–264.
57. Stone, G.W.; Liu, B.; Pepper, D.A.; Wang, P. The importance of extratropical and tropical cyclones on the short-term evolution of barrier islands along the northern Gulf of Mexico, USA. *Mar. Geol.* **2004**, *210*, 63–78.
58. Del Castillo, C.E. Remote sensing of organic matter in coastal waters. In *Remote Sensing of Coastal Aquatic Environments*; Springer: Berlin, Germany, 2005; pp. 157–180.
59. Miller, W.L.; Zepp, R.G. Photochemical production of dissolved inorganic carbon from terrestrial organic matter: Significance to the oceanic organic carbon cycle. *Geophys. Res. Lett.* **1995**, *22*, 417–420.
60. Moran, M.A.; Sheldon, W.M.; Zepp, R.G. Carbon loss and optical property changes during long-term photochemical and biological degradation of estuarine dissolved organic matter. *Limnol. Oceanogr.* **2000**, *45*, 1254–1264.
61. Osburn, C.L.; Retamal, L.; Vincent, W.F. Photoreactivity of chromophoric dissolved organic matter transported by the Mackenzie River to the Beaufort Sea. *Mar. Chem.* **2009**, *115*, 10–20.
62. Uher, G.; Hughes, C.; Henry, G.; Upstill-Goddard, R.C. Non-conservative mixing behavior of colored dissolved organic matter in a humic-rich, turbid estuary. *Geophys. Res. Lett.* **2001**, *28*, 3309–3312.
63. Kutser, T.; Pierson, D.C.; Kallio, K.Y.; Reinart, A.; Sobek, S. Mapping lake CDOM by satellite remote sensing. *Remote Sens. Environ.* **2005**, *94*, 535–540.
64. Moeller, C.C.; Huh, O.K.; Roberts, H.H.; Gumley, L.E.; Menzel, W.P. Response of Louisiana coastal environments to a cold front passage. *J. Coast. Res.* **1993**, *9*, 434–447.
65. D'Sa, E.J.; Miller, R.L. Bio-optical properties in waters influenced by the Mississippi River during low flow conditions. *Remote sens. Environ.* **2003**, *84*, 538–549.
66. Ward, L.G. The influence of wind waves and tidal currents on sediment resuspension in middle Chesapeake Bay. *Geo-Mar. Lett.* **1985**, *5*, 71–75.